ACS APPLIED MATERIALS & INTERFACES

Research Article

www.acsami.org

Catalyst-Free Synthesis of Si-SiO_x Core-Shell Nanowire Anodes for High-Rate and High-Capacity Lithium-Ion Batteries

Kwan Woo Lim,[†,§] Jung-In Lee,[†,§] Jieun Yang,[†] Young-Ki Kim,[‡] Hu Young Jeong,[‡] Soojin Park,*[,†] and Hyeon Suk Shin*[,†]

[†]Interdisciplinary School of Green Energy and Low Dimensional Carbon Materials Center, Ulsan National Institute of Science and Technology (UNIST), UNIST-gil 50, Ulsan 689-798, Republic of Korea

[‡]UNIST Central Research Facilities, Ulsan National Institute of Science and Technology (UNIST), UNIST-gil 50, Ulsan 689-798, Republic of Korea

Supporting Information

ABSTRACT: Si-SiO_x core-shell nanowires (NWs) ranging from 10 to 30 nm in diameter are prepared by a simple evaporation of silicon monoxide and control of substrate temperatures without any catalyst. The Si-SiO_x NWs grown at 735 and 955 °C are strongly anchored to the Cu current collector by forming copper silicide at the interface between Si and Cu, and subsequently used as anodes in lithium-ion batteries, in which no binder or conducting materials are used. The Si-SiO_x NWs anodes show excellent electrochemical performances in terms of capacity retention and rate capability. In particular, the Si-SiO_x NW anode grown at 955 °C shows a reversible capacity of ~1000 mAh g^{-1} even at a high-rate of 50 C. This catalyst-free synthetic route of Si-SiO_x NWs that are strongly anchored to the Cu current collector opens up an effective process for fabricating other high-capacity anodes in lithium-ion batteries (LIBs).

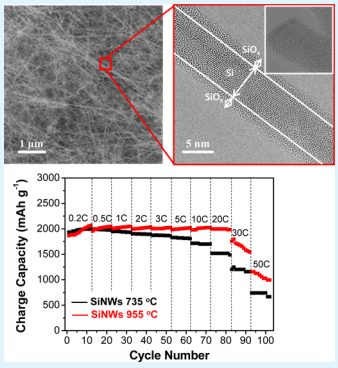

KEYWORDS: *silicon-based anode, silicon nanowire, silicon oxide, core/shell nanowire, lithium-ion battery, rate capability*

INTRODUCTION

Energy storage devices have been of great importance because of recent technology advancements such as portable electronics, smart grids, hybrid electric vehicles, and electric vehicles.[1] In particular, lithium-ion batteries (LIBs) using Si anodes have attracted much interest because their theoretical capacity, 3750 $mAhg^{-1}$ at room temperature, is 10 times higher than that of commercialized graphite, 372 $mAhg^{-1}$. Among various low-dimensional Si nanostructures including 0-dimensional (0D) nanoparticles,[2,3] 1D nanowires (NWs),[4−23] and 2D thin films,[2] 1D NWs are the most attractive for anode materials in LIBs. It is known that Si NWs can minimize the volume expansion due to strain relaxation and provide efficient electronic pathways.[6,9] In practice, the volume expansion of more than 300% of the Si during lithiation and delithiation causes fractures in the Si nanostructures, resulting in capacity loss in LIBs. However, even LIBs with Si NW anodes showed significantly high capacity fade upon charging/discharging due to serious aggregation of the Si NWs and the formation of an unstable solid electrolyte interface (SEI).[4,11]

To prevent this capacity fading in LIBs with Si NWs, several approaches have been developed including an amorphous carbon or carbon nanotube coating on the Si NWs' surfaces[1,4] or a core-shell design of the Si NWs.[6] The core-shell structure consists of crystalline Si in the core and an amorphous SiO_x layer in the shell, in which Si mainly contributes to the capacity of the LIB, while amorphous SiO_x accommodates a large volume change of the Si during cycling.[6] Thus, the core-shell structures can improve the capacity retention and cyclability of LIBs. For example, Cui's group has demonstrated excellent capacity retention in a LIB with Si (10 nm)-SiO_x (50 ± 10 nm) core-shell NWs. In their results, 90% of initial capacity (1000 mAh g^{-1}) remained after 100 cycles.[6]

Although much research on Si NWs anodes in LIBs has been carried out, there have been few reports on the NWs' diameter-dependent performance. It is only known that Si NWs with smaller diameters yield a higher specific capacity at various C rates.[9] Recently, it was reported that a native oxide layer at the surface of the NWs with a diameter of less than 50 nm efficiently prevented the volume expansion.[13] To improve performance of LIBs to the level required for commercialization in terms of cyclability and rate capability, therefore, we require further research on the capacity, cyclability, and rate capability of LIBs with Si-SiO_x core-shell NWs with diameters of less than 50 nm.

So far, many approaches to growing Si NWs have been developed: the vapor−liquid−solid (VLS) method,[12,13] vapor−solid (VS) method,[15,24] laser ablation (LA) method,[20,22] oxide-assisted growth (OAG) method,[19] and supercritical-fluid−solid−solid (SFSS) method.[4] The catalysts used for growth of

Received: December 6, 2013
Accepted: April 22, 2014
Published: April 22, 2014

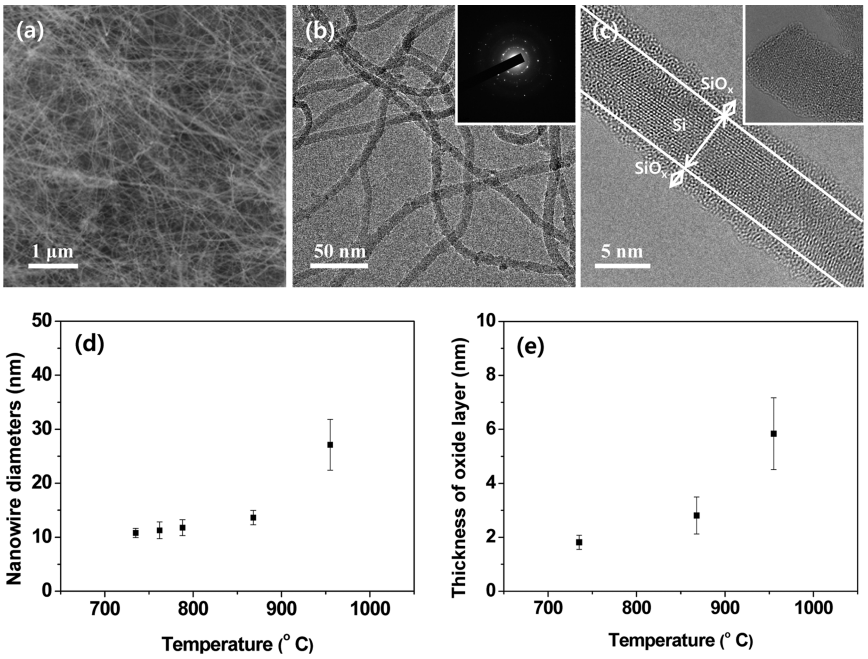

Figure 1. (a) SEM image of Si-SiO_x NWs grown on a Cu surface at 735 °C. (b) Low-magnification TEM image of Si-SiO_x NWs. The inset is an ED pattern of a wire indicating its polycrystalline nature. (c) HR-TEM image of Si-SiO_x NWs. The NW is composed of a Si core and a SiO_x shell. The inset shows the end of a single NW without any metal catalyst. (d) Plot of diameter of NWs vs temperature. (e) Plot of SiO_x shell thickness at one side vs temperature.

Si NWs in approaches such as the VLS method can be a source of contamination in NW-based devices that has a negative effect on performance of the device. In case of a LIB with Si NWs, a metal catalyst could result in reversible capacity loss due to a side reaction with the metal or electrical disconnection.[25] On the other hand, a simple vaporization process of a precursor such as the VS method can exclude any possibility of contamination, because it does not use any catalyst.

Herein, we report that diameter-controlled Si-SiO_x core-shell NWs with diameters in the range from 10 to 30 nm can be used for anode materials in LIBs. The diameter control of such small core-shell NWs has been realized by simply evaporating SiO powder and changing the substrate temperature without any catalyst. Since the growth of the core-shell NWs is not dependent on the type of substrate, they were directly grown on the copper foil used as the current collector in the LIB. Therefore, LIB cells could be fabricated without any metal catalyst, binder, or conducting materials, which excludes the possibility of contamination or side reactions. The LIBs showed excellent electrochemical performance: more than 95% of the initial delithiation capacity remained after 100 cycles. Moreover, the LIB with Si-SiO_x NWs grown at 955 °C showed excellent rate capabilities of ~2000 and ~1000 mAh g^{-1} at 20 and 50 C, respectively. This is possibly due to the very small Si-SiO_x core-shell NWs, since a small-diameter Si core strongly anchored to the current collector can effectively shorten the diffusion distance of the Li ions at high C rates and the SiO_x shell can efficiently prevent the volume expansion of the Si.

EXPERIMENTAL SECTION

Synthesis. Si-SiO_x NWs were directly grown on 25 μm thick copper foils without any catalyst by evaporation of SiO powder (Aldrich, 325 mesh) using thermal chemical vapor deposition (CVD). In the set-up for thermal CVD, the tube furnace consists of three independent heating zones, and thus, temperature of the substrate (copper foil) on a sample stage with thermocouple could be controlled by changing temperature of each heating zone (Supporting Information (SI), Figure S1). SiO powder (0.2 g) and the copper foil on the sample stage were placed in zone 1 and zone 3, respectively. Then, zone 1 and zone 2 were heated to 1100 °C in flow of Ar as a carrier gas at 65 sccm, and maintained at 1100 °C for 2 h. The temperature of the sample stage was controlled in the range from 735 to 955 °C by varying temperature of zone 3. Then, Si-SiO_x NWs with different diameter were obtained at different temperature of the sample stage, indicating that the substrate temperature acts as a critical factor for the diameter control in our study.

Characterization. The morphology and diameter of Si-SiO_x NWs were characterized with a scanning electron microscope (SEM, Nanonova 230, FEI), a high-resolution transmission electron microscope (HR-TEM, JEM-2100F, JEOL), a Raman spectrometer (Alpha 300R, WITec), and an X-ray diffractometer (D/MAZX 2500 V/PC, Rigaku; 18 kW Cu target as the source and 0.154 nm of Cu Kα radiation).

Electrochemical Test. For the electrochemical test, coin type half-cells (2016R type) that were composed of the SiNWs directly grown on the Cu current collector as the working electrode and lithium metal as both reference and counter electrodes were fabricated in an argon-filled glove box. Binders and conducting carbon were not used due to the direct contact of the active materials to the current collector. Separators from celgard (Celgard 2400 microporous membrane, polypropylene) were used. The electrolyte was a commercial solution of 1.3 M $LiPF_6$ in ethylene carbonate/diethyl carbonate (Panaxetech, EC/DEC, 30:70 vol %) with additive as 5 wt % fluoroethylene carbonate (FEC). All cells were cycled at a rate of 0.1-50 C between 0.005 and 1.2 V. The lithiation/delithiation rate is calculated based on theoretical capacity at room temperature (25 °C), corresponding to 1 C = 3.7 A g^{-1}. After cycling, we disassembled cells in the glove box. The cycled electrodes were rinsed with DMC to remove a residual $LiPF_6$ based electrolyte. Electrochemical Impedance Spectroscopy (EIS) measurements were conducted on (BioLogic, National Instruments). The impedance was measured before and after first cycle. The typical frequency range was between 100 kHz to 100 mHz and the applied AC voltage was 10 mV.

dx.doi.org/10.1021/am405618m | ACS Appl. Mater. Interfaces 2014, 6, 6340−6345

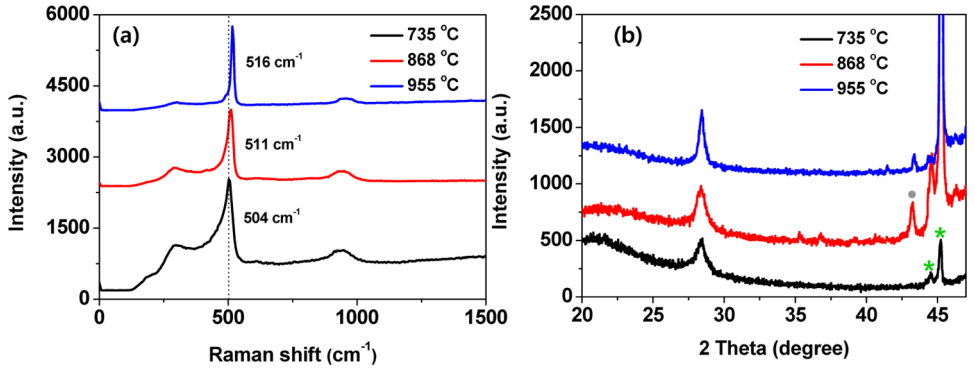

Figure 2. (a) Raman spectrum of Si-SiO_x NWs at each temperature: 735 °C, black; 868 °C, red; and 955 °C, blue. (b) XRD spectrum of Si-SiO_x NWs at each temperature: 735 °C, black; 868 °C, red; 955 °C, blue. The asterisk (*) indicates Cu_3Si and the circle (●) shows $Cu_{15}Si_4$.

RESULTS AND DISCUSSION

The growth of Si NWs by thermal evaporation of SiO powder using thermal CVD with three heating zones is affected by many parameters such as the working pressure, evaporation temperature of the precursors, argon (Ar) flow rate, and substrate temperature. Then, the substrate temperature was changed in the range from 735 to 955 °C. (see Supporting Information, Figure S1) As a result, uniform and dense Si-SiO_x NWs were grown on the surfaces of Cu foils, and their diameter was dependent on the substrate temperature. Note that no metal or nonmetal catalyst was used in the growth of the Si-SiO_x NWs, and their diameter could be controlled in the range of around 10 to 30 nm.

Figure 1a shows a SEM image of the NWs grown on Cu foil for 2 h at a substrate temperature of 735 °C. This image confirms that dense NWs with lengths of tens of micrometers were grown on the Cu surface. Figure 1b shows a low-magnification TEM image that confirms the uniformity of the NWs. The electron diffraction (ED) pattern in the inset of Figure 1b, which was measured from a single NW, indicates that the NWs are polycrystalline. The HR-TEM image in Figure 1c verifies that the NWs are core-shell structures consisting of a polycrystalline Si core and an amorphous SiO_x shell. The same phenomena were observed for NWs grown at 868 and 955 °C (SI, Figure S2). We also confirmed from the inset of Figure 1c that there is no metal catalyst at the ends of the NWs, which is a result of the catalyst-free synthetic route. Furthermore, since the growth of the Si-SiO_x core-shell NWs was successful on Si and sapphire substrates, the method is not dependent on the type of substrate (SI, Figure S3 and S4). Note that stoichiometry of Si and O in the shell could not be determined due to variation of atomic ratio of Si and O in EDX results of HR-TEM at different samples (SI, Figure S5).

The average diameter of the Si-SiO_x NWs grown at different substrate temperatures was measured from HR-TEM images. About 20 NWs per sample were used for calculation of the average diameter, which included both the core and shell parts, and the SiO_x shell thickness at one side of the NWs (Figure 1d and e). At a substrate temperature of 735 °C, the average diameter of the Si-SiO_x NWs and the shell thickness are 10.8 ± 0.9 and 1.8 ± 0.3 nm, respectively. Thus, the Si core is estimated to be around 7 nm in diameter. Meanwhile, at a substrate temperature of 868 °C, the average diameter and shell thickness are 13.7 ± 1.3 and 2.8 ± 0.7 nm, respectively, corresponding to an Si core of around 8 nm in diameter, and at a substrate temperature of 955 °C, they are 27.1 ± 4.7 and 5.8 ± 1.3 nm, respectively, corresponding to an Si core of around 16 nm in diameter. As the substrate temperature increases, both the diameter and the shell thickness increase. This suggests that we can tune the diameter of the NWs by simply changing the substrate temperature. So far, diameter control of Si NWs has been achieved by changing the thickness of the Au catalyst film,[9] by changing the size of the gold catalyst nanoclusters,[26] by changing the ambient pressure,[27] and by performing laser ablation in different ambient gases.[21]

The growth of the Si-SiO_x NWs can be understood as an oxide-assisted growth mechanism.[28] However, the growth mechanism of the NWs is not obvious yet because forming Si NWs (or Si-SiO_x NWs in this study) by evaporating SiO is a complicated process and not fully understood, and thus further study is required.[29] In fact, even though Si-SiO_x core-shell NWs have been grown by evaporating SiO powder and controlled by substrate temperature previously, the reported growth results were different from ours. For example, Au catalyst was still necessary to grow the NWs,[12] or the NWs were not grown at a substrate temperature range similar to that used in our study.[29] Based on these previous reports, we recognize that the growth of NWs from evaporated SiO is very sensitive to the experimental conditions such as the evaporation temperature, working pressure, carrier gas flow, and substrate temperature. In this study, the occurrence of the disproportionation reaction of SiO to give Si and SiO_2 seems to be feasible during the evaporation of SiO.[12]

Figure 2a shows the Raman spectra of Si-SiO_x NWs obtained at different substrate temperatures. The position of the band due to the F_{2g} mode increased in wavenumber as the substrate temperature increased: it was 504 cm^{-1} at 735 °C, 511 cm^{-1} at 868 °C, and 516 cm^{-1} at 955 °C. Note that the bandwidth of the F_{2g} mode arising from scattering of the first-order optical phonon of crystalline Si becomes broad and the band position shifts toward lower frequencies as the diameter of the Si NW decreases.[16] Furthermore, it was found that the changes in the band are due to the phonon confinement effect, which becomes more obvious in Si NWs with diameters less than 22 nm.[16] This result is consistent with our Raman spectra for core-shell NWs with such small diameters. In addition, the XRD spectra in Figure 2b confirm the existence of a crystalline Si core. As the substrate temperature increases, the full width at half maximum of the Si (111) peak at 28.4° decreases and the peak width decreases, indicating the increase in the crystallinity of Si at high substrate temperatures.

The electrochemical performance of the Si-SiO_x NWs (loading mass = ~0.5 mg/cm^2) grown at 735 °C and 955 °C

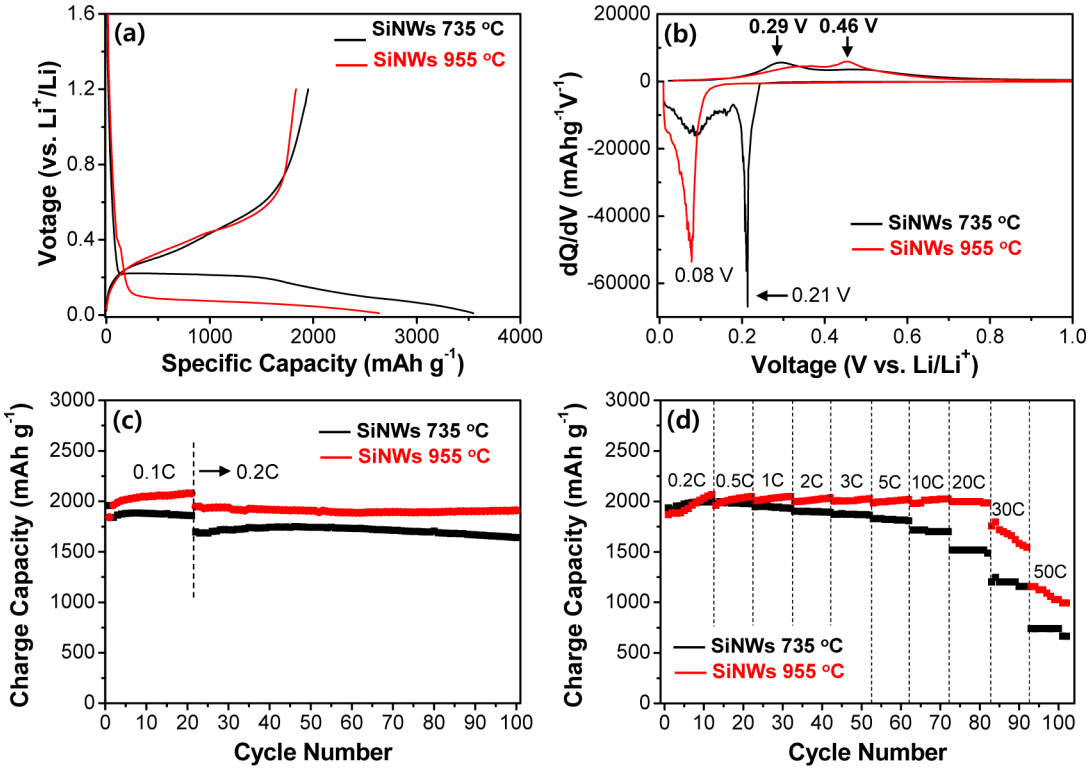

Figure 3. Electrochemical properties of Si-SiO_x NW electrodes grown at a substrate temperature of 735 °C and Si-SiO_x NW electrodes grown at a substrate temperature of 955 °C. (a) First discharging and charging cycles of both electrodes at a 0.1 C rate in the range of 0.005−1.2 V. (b) dQ/dV plots of the voltage profiles seen in part a. (c) Cycle retention of both Si NW electrodes at 0.1 and 0.2 C rates. (d) Rate capabilities of both electrodes at various C rates. The discharge rate was fixed to 0.2 C.

was evaluated using galvanostatic discharging and charging between 0.005 and 1.2 V in 2016 coin half-cells with lithium counter electrode. The first cycle discharge and charge capacities of the Si-SiO_x NWs-735 electrode (NWs grown at a substrate temperature of 735 °C) at a 0.1 C rate are 3545 and 1868 $mAhg^{-1}$, corresponding to a low coulombic efficiency of 55%, while the Si-SiO_x NWs-955 electrode (NWs grown at substrate temperature of 955 °C) showed an initial discharge capacity of 2633 $mAhg^{-1}$ with a coulombic efficiency of 69% (Figure 3a). The low coulombic efficiency of the Si-SiO_x NWs is attributed to the formation of Li_2O and lithium silicate (both inactive materials) during the lithiation of the SiO_x shell layers. In particular, the voltage profiles of the Si-SiO_x NWs-735 electrode look like those of typical amorphous silicon monoxide (SiO) anodes.[30] The differential capacity (dQ/dV) plots of both NW anodes more clearly show the characteristics of the SiO_x shell layers (Figure 3b). In the case of the Si-SiO_x NWs-735 electrode, an intense peak was observed at 0.21 V during the first lithiation (discharging) process. This peak may be caused by the formation of lithium silicate and Li_2O during the first lithiation (discharging) of SiO, as previously reported.[31] During the first lithiation (discharging), a broad peak was seen between 0.12 and 0.08 V due to the phase transition between amorphous Li_xSi phases.[32] Conversely, during the delithiation (charging) process, the broad peaks at 0.29 and 0.46 V are assignable to a reversible reaction occurring in the amorphous Si electrodes.[33] However, the peak appearing at ∼0.21 V seen in the Si-SiO_x NWs-735 profile was not seen for Si-SiO_x NWs-955, indicating that there was significantly less formation of Li_2O and lithium silicate for Si-SiO_x NWs-955 than for Si-SiO_x NWs-735 (Figure 3b). It may lead to the increase of initial coulombic efficiency of the samples grown at 955 °C. Both Si-SiO_x NW electrodes showed highly stable cycling up to 100 cycles at 0.1−0.2 C rates (Figure 3c). At the 0.2 C rate, the Si-SiO_x NWs-735 and Si-SiO_x NWs-955 electrodes showed high reversible capacities of 1640 and 1910 $mAhg^{-1}$, respectively, with excellent capacity retention of more than 95% of the initial capacity. The existence of SiO_x outer layers in the Si-SiO_x NWs lowers the initial coulombic efficiency by allowing the formation of Li_2O and lithium silicate. However, the SiO_x layer can mitigate the large volume change of the Si core during the lithiation/delithiation process, resulting in highly stable cycling performance. Electrochemical properties of other nanostructured Si anodes with SiO_x native oxide layers were compared with our results (SI, Table S1).

Moreover, the rate capabilities of the Si-SiO_x NWs electrodes were investigated at various C rates (0.2−50 C) between 1.2 and 0.005 V in a coin-type half-cell (Figure 3d). Note that the discharge (lithiation) was fixed at a rate of 0.2 C. The Si-SiO_x NWs-955 electrode showed a specific capacity of ∼2000 $mAhg^{-1}$ at a high rate of 20 C, which is similar to that obtained at the 0.2 C rate. Even at the high rate of 50 C, the specific capacity was ∼1000 $mAhg^{-1}$, which is about 3 times higher than that of carbon-based electrodes. In contrast, the Si-SiO_x NWs-735 electrode yielded slightly lower reversible capacities at the various rates as compared to those of the NWs grown at 955 °C. However, it still showed a high rate capability, exhibiting specific capacities of 1735, 1200, and 750 mAh g^{-1} at 20, 30, and 50 C rates, respectively. These high rate capabilities can be explained as follows. First, the Si-SiO_x NWs were strongly anchored to the current collector, so that all NWs could contribute to the capacity. We could observe the

dx.doi.org/10.1021/am405618m | ACS Appl. Mater. Interfaces 2014, 6, 6340−6345

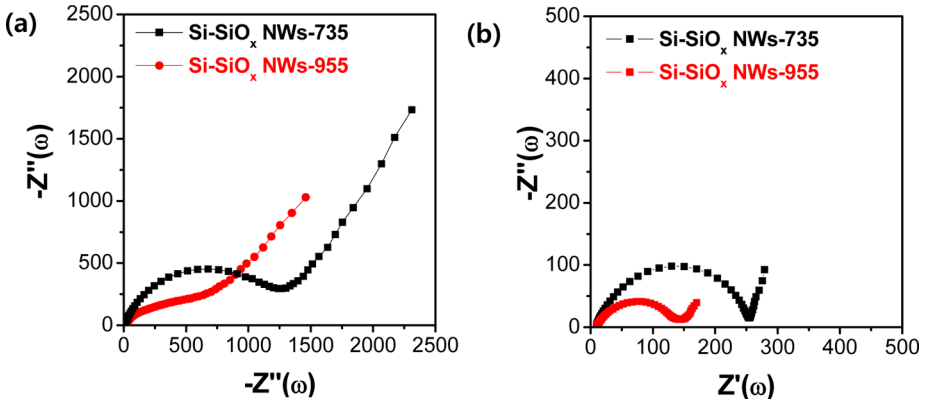

Figure 4. Electrochemical impedance spectra points from the Si-SiO_x NWs-735 and Si-SiO_x NWs-955 electrodes (a) after first cycle and then (b) at lithiated state of 0.01 V.

formation of copper silicide from XRD spectrum, indicating that the Si-SiO_x NWs were synthesized with strong binding to the current collector (Figure 2b). In fact, several studies concerning the direct contact of electrodes to the current collector have been reported confirming this effect.[34,35] Second, the 1D Si NWs allow efficient charge transport through the 1D electronic pathways. Third, lithium ions and electrolytes can easily access NWs electrodes with sub-30 nm diameters.

To further explain the rate capability, the Nyquist plot provides information related to the surface resistance of the electrodes and the solid-state diffusion of lithium ions.[36] The semicircle at the high-frequency range (between 100 kHz and 10 Hz) indicates the surface resistance of the Si-SiO_x NWs due to the electron transfer resistance at the electrode interface and SEI layer. At lower frequencies (below 10 Hz), the contribution from solid-state diffusion as lithium ions move into the bulk of the Si NW is seen.[37] The interfacial resistances (i.e., the semicircle size) of the Si-SiO_x NWs-955 electrodes were much lower than those of the Si-SiO_x NWs-735 electrodes at all points (Figure 4). These results can be explained as follows. First, the crystallinity of the Si core is different in the Si-SiO_x NWs grown at different substrate temperatures. It is well known that the electrical conductivity of Si increases with its crystallinity.[38] As shown in Figure 2, the crystallinity of the Si grown at 955 °C is higher than that of the Si grown at 735 °C. Therefore, the Si-SiO_x NWs-955 electrode showed superior rate performance to that of the S-SiO_x NWs-735 electrode. Second, the SiO_x shell layers affect the surface resistance of the Si-SiO_x NWs electrodes. The electrochemical properties of the Si-SiO_x NWs grown at low temperatures look similar to those of the SiO anodes. As indicated in Figure 3b, the reaction between the Si-SiO_x NWs-735 electrode and the lithium ions formed large amounts of Li_2O and lithium silica during the first lithiation process, resulting in an increase in the surface resistance, while these results were not observed in the Si-SiO_x NWs-955 electrode. Third, because of its large surface area compared to that of the Si-SiO_x NWs-955 electrode, a significant side reaction might occur on the surface of the Si-SiO_x NWs-735 electrode after five cycles. However, the observed dimensions of both types of Si NWs (after 5 cycles) were quite similar to those of the original Si NWs (SI, Figure S6). The crystallinity of the Si, the characteristics of the SiO_x shell, and the dimensions of the Si NWs all play important roles in improving the cycling performance and rate capability of Si-SiO_x NWs electrodes.

CONCLUSION

In summary, we successfully synthesized sub-30 nm Si-SiO_x core-shell NWs on various substrates by simply evaporating SiO powder without any catalyst. When the Si-SiO_x NWs were grown on Cu foil that could act as a current collector, the NWs were strongly anchored to the Cu foil and could be used as anode materials in LIBs without any binder or conducting material. The Si-SiO_x NW anodes exhibited excellent electrochemical performance including a high reversible capacity (~2000 $mAhg^{-1}$ at a 0.2 C rate), a high rate capability (1000 $mAhg^{-1}$ at 50 C rate), and a highly stable cycling retention (>95% after 100 cycles, compared to the initial capacity). This simple catalyst-free synthetic process for producing Si-SiO_x NWs provides an effective way to prepare high-performance anode materials for LIBs.

ASSOCIATED CONTENT

Supporting Information

Experimental procedure, SEM and HR-TEM images of NWs grown at different substrate temperatures, and SEM images of NWs grown on different substrates. This material is available free of charge via the Internet at http://pubs.acs.org.

AUTHOR INFORMATION

Corresponding Authors

*Email: spark@unist.ac.kr.
*Email: shin@unist.ac.kr.

Author Contributions

§K.W.L. and J.-I.L. contributed equally.

Notes

The authors declare no competing financial interest.

ACKNOWLEDGMENTS

This work was supported by a grant (Code No. 2011-0031630) from the Center for Advanced Soft Electronics under the Global Frontier Research Program through the National Research Foundation funded by the Ministry of Science, ICT, and Future Planning and by the BK21 Plus program (META-material-based Energy Harvest and Storage Technologies, 10Z20130011057) funded by the Ministry of Education, Korea.

REFERENCES

(1) Huang, R.; Fan, X.; Shen, W.; Zhu. Carbon-Coated Silicon Nanowire Array Films for High Performance Lithium-Ion Battery Anodes. *J. Appl. Phys. Lett.* **2009**, *95*, 133119.

(2) Kasavajjula, U.; Wang, C.; Appleby, A. J. Nano-and Bulk-Silicon-Based Insertion Anodes for Lithium-Ion Secondary Cells. *J. Power Sources* **2007**, *163*, 1003−1039.
(3) Kim, I. S.; Kumta, P. N. High Capacity Si/C Nanocomposite Anodes for Li-Ion Batteries. *J. Power Sources* **2004**, *136*, 145−149.
(4) Chan, C. K.; Patel, R. N.; O'Connell, M. J.; Korgel, B. A.; Cui, Y. Solution-Grown Silicon Nanowires for Lithium-Ion Battery Anodes. *ACS Nano* **2010**, *4*, 1443−1450.
(5) Chockla, A. M.; Harris, J. T.; Akhavan, V.A.; Bogart, T. D.; Holmberg, V. C.; Steinhagen, C.; Mullins, C. B.; Stevenson, K. J.; Korgel, B. A. Silicon Nanowire Fabric as a Lithium Ion Battery Electrode Material. *J. Am. Chem. Soc.* **2011**, *133*, 20914−20921.
(6) Cui, L. F.; Ruffo, R.; Chan, C. K.; Peng, H.; Cui, Y. Crystalline-Amorphous Core-Shell Silicon Nanowires for High Capacity and High Current Battery Electrodes. *Nano Lett.* **2008**, *9*, 491−495.
(7) Cui, Y.; Wei, Q.; Park, H.; Lieber, C. M. Nanowire Nanosensors for Highly Sensitive and Selective Detection of Biological and Chemical Species. *Science* **2001**, *293*, 1289−1292.
(8) Cui, Y.; Zhong, Z.; Wang, D.; Wang, W. U.; Lieber, C. M. High Performance Silicon Nanowire Field Effect Transistors. *Nano Lett.* **2003**, *3*, 149−152.
(9) Gohier, A.; Laïk, B.; Pereira-Ramos, J. P.; Cojocaru, C. S.; Tran-Van, P. Influence of the Diameter Distribution on the Rate Capability of Silicon Nanowires for Lithium-Ion Batteries. *J. Power Sources* **2012**, *203*, 135−139.
(10) Huang, Y.; Duan, X.; Cui, Y.; Lauhon, L. J.; Kim, K. H.; Lieber, C. M. Logic Gates and Computation from Assembled Nanowire Building Blocks. *Science* **2001**, *294*, 1313−1317.
(11) Kang, K.; Lee, H.-S.; D.-W; Kim, G.-S.; Lee, D.; Lee, G.; Kang, Y.-M.; Jo, M.-H. Maximum Li Storage in Si Nanowires for the High Capacity Three-Dimensional Li-Ion Battery. *Appl. Phys. Lett.* **2010**, *96*, 053110.
(12) Kolb, F. M.; Hofmeister, H.; Scholz, R.; Zacharias, M.; Gosele, U.; Ma, D. D.; Lee, S. T. Analysis of Silicon Nanowires Grown by Combining SiO Evaporation with the VLS Mechanism. *J. Electrochem. Soc.* **2004**, *151*, G472−G475.
(13) McDowell, M. T.; Lee, S. W.; Ryu, I.; Wu, H.; Nix, W. D.; Choi, J. W.; Cui, Y. Novel Size and Surface Oxide Effects in Silicon Nanowires as Lithium Battery Anodes. *Nano Lett.* **2011**, *11*, 4018−4025.
(14) Q Peng, K.; P Huang, Z.; Zhu, J. Fabrication of Large-Area Silicon Nanowire p−n Junction Diode Arrays. *Adv. Mater.* **2004**, *16*, 73−76.
(15) Qin, Y.; Zhang, X. N.; Zheng, K.; Li, H.; Han, X. D.; Zhang, Z. Unusual Catalyst-Free Epitaxial Growth of Silicon Nanowires by Thermal Evaporation. *Appl. Phys. Lett.* **2008**, *93*, 063104.
(16) Wang, R.; Zhou, G.; Liu, Y.; Pan, S.; Zhang, Z. Raman Spectral Study of Silicon Nanowires: High-Order Scattering and Phonon Confinement Effects. *Phys. Rev. B* **2000**, *61*, 16827−16832.
(17) Yao, Y.; Li, F.; Lee, S. T. Oriented Silicon Nanowires on Silicon Substrates from Oxide-Assisted Growth and Gold Catalysts. *Chem. Phys. Lett.* **2005**, *406*, 381−385.
(18) Yu, D. P.; Bai, Z. G.; Ding, Y.; Hang, Q. L.; Zhang, H. Z.; Wang, J. J.; Zou, Y. H.; Qian, W.; Xiong, G. C.; Zhou, H. T.; Feng, S. Q. Nanoscale Silicon Wires Synthesized Using Simple Physical Evaporation. *Appl. Phys. Lett.* **1998**, *72*, 3458−3460.
(19) Zhang, R. Q.; Lifshitz, Y.; Lee, S. T. Oxide-Assisted Growth of Semiconducting Nanowires. *Adv. Mater.* **2003**, *15*, 635−640.
(20) Zhang, Y.; Tang, Y.; Wang, N.; Lee, C.; Bello, I.; Lee, S. One-Dimensional Growth Mechanism of Crystalline Silicon Nanowires. *J. Cryst. Growth* **1999**, *197*, 136−140.
(21) Zhang, Y. F.; Tang, Y. H.; Peng, H. Y.; Wang, N.; Lee, C. S.; Bello, I.; Lee, S. T. Diameter Modification of Silicon Nanowires by Ambient Gas. *Appl. Phys. Lett.* **1999**, *75*, 1842−1844.
(22) Zhang, Y. F.; Tang, Y. H.; Wang, N.; Yu, D. P.; Lee, C. S.; Bello, I.; Lee, S. T. Silicon Nanowire Prepared by Laser Ablation at High Temperature. *Appl. Phys. Lett.* **1998**, *72*, 1835−1837.
(23) Kim, B. S.; Koo, T. W.; Lee, J. H.; Kim, D. S.; Jung, Y. C.; Hwang, S. W.; Choi, B. L.; Lee, E. K.; Kim, J. M.; Whang, D. Catalyst-Free Growth of Single-Crystal Silicon and Germanium Nanowires. *Nano Lett.* **2009**, *9*, 864−869.
(24) Park, M.-S.; Wang, G.-X.; Kang, Y.-M.; Wexler, D.; Dou, S.-X.; Liu, H.-K. Preparation and Electrochemical Properties of SnO_2 Nanowires for Application in Lithium-Ion Batteries. *Angew. Chem. Int. Ed.* **2007**, *46*, 750−753.
(25) Chen, X.; Ruoff, R. S. Simple and Catalyst-Free Synthesis of Silicon Oxide Nanowire and Nanocoils. *Nano* **2007**, *02*, 91−95.
(26) Cui, Y.; Lauhon, L. J.; Gudiksen, M. S.; Wang, J.; Lieber, C. M. Diameter-Controlled Synthesis of Sincle-Crystal Silicon Nanowires. *Appl. Phys. Lett.* **2001**, *78*, 2214−2216.
(27) Zhang, H. Z.; Yu, D. P.; Ding, Y.; Bai, Z. G.; Hang, Q. L.; Feng, S. Q. Dependence of the Silicon Nanowire Diameter on Ambient Pressure. *Appl. Phys. Lett.* **1998**, *73*, 3396−3398.
(28) Lee, S. T.; Wang, N.; Zhang, Y. F.; Tang, Y. H. Oxide-Assisted Semiconductor Nanowire Growth. *Mater. Res. Bull.* **1999**, *24*, 36−42.
(29) Pan, Z. W.; Dai, Z. R.; Xu, L.; Lee, S. T.; Wang, Z. L. Temperature-Controlled Growth of Silicon-Based Nanostructures by Thermal Evaporation of SiO powders. *J. Phys. Chem. B* **2001**, *105*, 2507−2514.
(30) Lee, J.-I.; Choi, N.-S.; Park, S. Highly Stable Si-Based Multicomponent Anodes for Practical Use in Lithium-Ion Batteries. *Energy Environ. Sci.* **2012**, *5*, 7878−7882.
(31) Kim, T.; Park, S.; Oh, S. M. Solid-State NMR and Electrochemical Dilatometry Study on Li^+ Uptake/Extraction Mechanism in SiO Electrode Batteries and Energy Storage. *J. Electrochem. Soc.* **2007**, *154*, A1112−A1117.
(32) Li, J.; Dahn, J. R. An In Situ X-Ray Diffraction Study of the Reaction of Li with Crystalline Si Batteries and Energy Storage. *J. Electrochem. Soc.* **2007**, *154*, A156−A161.
(33) Obrovac, M. N.; Christensen, L. Structural Changes in Silicon Anodes during Lithium Insertion/Extraction. *Electrochem. Solid-State Lett.* **2004**, *7*, A93−A96.
(34) Chan, C. K.; Peng, H.; Liu, G.; McIlwrath, K.; Zhang, X. F.; Huggins, R. A.; Cui, Y. High-Performance Lithium Battery Anodes Using Silicon Nanowires. *Nat. Nanotechnol.* **2008**, *3*, 31−35.
(35) Taberna, P. L.; Mitra, S.; Poizot, P.; Simon, P.; Tarascon, J.-M. High Rate Capabilities Fe_3O_4-based Cu Nano-Architectured Electrodes for Lithium-Ion Battery Applications. *Nat. Mater.* **2006**, *5*, 567−573.
(36) Barsoukov, E.; Macdonald, J. R. In *Impedance Spectroscopy: Theory, Experiment, and Applications*; John Wiley & Sons, Inc.: Hoboken, NJ, 2005, 444−468.
(37) Ruoff, R.; Hong, S. S.; Chang, C. K.; Huggins, R. A.; Cui, Y. Impedance Analysis of Silicon Nanowire Lithium Ion Battery Anodes. *J. Phys. Chem. C* **2009**, *113*, 11390−11398.
(38) Pinto, N.; Ficcadenti, M.; Morresi, L.; Murri, R.; Ambrosone, G.; Coscia, U. J. Electrical Transport Properties of Microcrystalline Silicon Grown by Plasma Enhanced Chemical Vapor Deposition. *J. Appl. Phys.* **2004**, *96*, 7306−7311.